Published in final edited form as:

Cancer Res. 2022 June 15; 82(12): 2313–2326. doi:10.1158/0008-5472.CAN-21-4145.

NR2F1 is a barrier to dissemination of early stage breast cancer cells

Carolina Rodriguez-Tirado[1,2,&],

Nupura Kale[1,2,3,&],

Maria J. Carlini[1,2,4],

Nitisha Shrivastava[1,2,5],

Alcina A. Rodrigues[1,2],

Bassem Khalil[2,6,7],

Jose J. Bravo-Cordero[2,6],

Yan Hong[8],

Melissa Alexander[9],

Jiayi Ji[2,10,11],

Fariba Behbod[8],

Maria S. Sosa[1,2,*]

[1]Department of Pharmacological Sciences, Icahn School of Medicine at Mount Sinai, New York, NY, 10029, USA.

[2]Tisch Cancer Institute, Icahn School of Medicine at Mount Sinai, New York, NY, 10029, USA.

[3]Present address: UCSF Helen Diller Comprehensive Family Cancer Center, University of California, San Francisco, CA, 94158, USA

[4]Present address: Columbia University, NY, 10027, USA

[5]Present address: Department of Pathology, Albert Einstein College of Medicine, Bronx, NY, 10461, USA.

[6]Division of Hematology and Oncology, Department of Medicine, Icahn School of Medicine at Mount Sinai, New York, NY, 10029, USA.

[7]Present address: Western Atlantic University School of Medicine, Plantation FL, USA 33324

[8]Department of Pathology and Laboratory Medicine, University of Kansas Medical Center, Kansas City, USA.

[9]Department of Anatomic Pathology, Icahn School of Medicine at Mount Sinai, New York, NY, 10029, USA.

[*]***Correspondence:*** Maria Soledad Sosa, Department of Pharmacological Sciences, Icahn School of Medicine at Mount Sinai, New York, NY, 10029, USA. Phone: 212-241-7135. maria.sosa@mssm.edu.

[&]:Equal contribution

The authors declare no potential conflicts of interest.

[10]Department of Population Health Science and Policy, Icahn School of Medicine at Sinai, New York, NY, 10029, USA.

[11]Present address: Rutgers University, NJ, 08854.

Abstract

Cancer cells can disseminate during very early and sometimes asymptomatic stages of tumor progression. Though biological barriers to tumorigenesis have been identified and characterized, the mechanisms that limit early dissemination remain largely unknown. We report here that the orphan nuclear receptor NR2F1/COUP-TF1 serves as a barrier to early dissemination. NR2F1 expression was decreased in patient ductal carcinoma in situ (DCIS) samples. High-resolution intravital imaging of HER2+ early stage cancer cells revealed that loss of function of NR2F1 increased in vivo dissemination and was accompanied by decreased E-cadherin expression, activation of WNT-dependent β-catenin signaling, disorganized laminin 5 deposition, and increased expression of EMT genes such as TWIST1, ZEB1, and PRRX1. Furthermore, downregulation of NR2F1 promoted a hybrid luminal/basal phenotype. NR2F1 expression was positively regulated by p38α signaling and repressed by HER2 and WNT4 pathways. Lastly, early cancer cells with NR2F1LOW/PRRX1HIGH staining were observed in DCIS samples. Together, these findings reveal the existence of an inhibitory mechanism of dissemination regulated by NR2F1 in early stage breast cancer cells.

Significance: During early stages of breast cancer progression, HER2-mediated suppression of NR2F1 promotes dissemination by inducing EMT and a hybrid luminal/basal-like program.

INTRODUCTION

Accumulating evidence in experimental models and human specimens across different cancers supports that early in cancer evolution, cancer cells disseminate to different anatomical sites[1-11]. For instance, patients with breast ductal carcinoma in situ (DCIS) lesions, defined by pathologists as non-invasive, carry early disseminated cancer cells (eDCCs) in target organs[5]. Interestingly, a small but significant percentage of women with DCIS who never progressed to an in-breast invasive disease died from a distant recurrence[8, 12], suggesting that eDCCs can fuel the formation of metastatic events[6, 7]. However, the mechanisms by which early cancer cells (ECCs) acquire motile and invasive features that allow dissemination and target organ colonization are not clearly understood.

We previously showed that early activation of the rat *Erbb2* (erb-b2 receptor tyrosine kinase) oncogene in mammary epithelial cells in young 14-18-week-old MMTV-HER2 females induced dissemination by turning off p38α/β signaling and promoting a Wnt-dependent partial EMT program[7]. Furthermore, we showed that upregulation of p38α/β signaling in dormant epithelial cancer cells (e.g. head and neck squamous cell carcinoma, HNSCC) could restore the expression of a member of the steroid hormone receptor family, NR2F1 (nuclear receptor subfamily 2, group F, member 1) [13, 14]. NR2F1 levels were downregulated in early lesions and primary tumors from the MMTV-HER2 mouse model and also in a HER2-independent MMTV-Myc model when compared to wild-type

siblings[13]. It is unclear whether the loss of NR2F1 in the case of HER2+ early lesions is linked to tumor suppression, early dissemination or both.

Here, we show that in murine and human early mammary cancer lesions, HER2 signaling reduced NR2F1 expression in a p38α-dependent manner. We also demonstrate that NR2F1 downregulation in HER2+ ECCs resulted in disorganized laminin V, reduced E-cadherin expression, activation of WNT (wingless-type MMTV integration site family, member 1)-dependent β-catenin signaling pathway as well as gain of a hybrid luminal/basal phenotype. Importantly, NR2F1 depletion in HER2+ ECCs also induces a partial EMT program. We also show using high-resolution intravital two-photon microscopy that loss of NR2F1 in MMTV-HER2 ECCs favors *in vivo* motility and invasion without increasing cancer cell proliferation. Lastly, we report an enrichment of pre-malignant cells with inverse correlation between NR2F1 and PRRX1 (paired related homeobox 1) expression levels ($NR2F1^{LOW}$/$PRRX1^{HIGH}$) in DCIS samples. We conclude that early in cancer evolution, NR2F1 serves as a barrier to dissemination of ECCs by repressing a partial EMT and a hybrid luminal/basal program triggered by HER2 signaling. These studies provide novel insight into early changes in cancer progression that may result in early metastatic seeding.

MATERIALS AND METHODS.

Animals and Cell Lines.

Animal procedures were approved by the Institutional Animal Care and Use Committee (IACUC) of Icahn School of Medicine at Mount Sinai protocol IACUC-2017-0162 and PROTO202100033. C57BL/6J *MKK3*$^{-/-}$/*MKK6*$^{+/-}$ and MMTV-HER2-CFP and MMTV-HER2 mice were previously described[7, 15]. FVB/N- Tg(MMTVneu)202Mul/J, nude ($FOXN1^{nu}$, RRID:IMSR_JAX:002376), wild type C57BL/6J (RRID:IMSR_JAX:000664) and FVB/NJ (RRID:IMSR_JAX:001800) animals were purchased from Jackson Laboratories. MMTV-rtTA-TetO-Neu mice[16, 17] were donated by Dr. Emily Bernstein (Icahn School of Medicine at Mount Sinai, NY, NY). Human MDA-MB-261 (RRID:CVCL_0179) and BT474 cell (RRID:CVCL_5593) lines were donated by Dr. Mihaela Skobe at Icahn School of Medicine at Mount Sinai and used between passages P3-P8. Mycoplasma testing (ATCC #30-1012K) was performed when cells were received on January 2021. SUM225 human cell line (RRID:CVCL_5593) was donated by Dr. Fariba Behbod at University of Kansas Medical Center and used between passages P99-P106. Mycoplasma testing was perform before shipping at Dr. Behbod lab, with date September, 2020.

Generation of MMTV-HER2 ECC cultures.

For generation of MMTV-HER2 early cancer cells (ECCs) cultures, we freshly isolated mammary epithelial cells from MMTV-HER2 females of 14-18 weeks of age which do not have any visible small lesions or palpable tumors among all 5 pairs of mammary glands as we have previously established in this model[7]. MMTV-HER2 mice were euthanized using CO_2 inhalation at 14-18 weeks of age. Whole mammary glands were minced and digested in Collagenase/BSA at 37°C for 45-60min. Red blood cell lysis buffer was used to remove blood cells and cells were then plated for 10-15min in DMEM+10%FBS in 100mm

dishes at 37°C for fibroblast removal. Cells were then incubated in 1mM PBS-EDTA for 15min at 37°C and passed through a 25-gauge needle. Cell suspensions were filtered through a 70 μm filter before counting. For generation of mammosphere cultures, isolated cells were seeded in 6-well ultra-low adhesion plates (Corning #3471) at a density of $1x10^6$ cells per well in 1.5 ml mammosphere medium [DMEM/F12 (Gibco #11320-082), 1:50 B27 Supplement (Gibco #17504-044), EGF (10 ng/ml; Peprotech #AF-100- 15-A), 1:100 Pen/Strep (Invitrogen #15070-06)]. The following day another 0.5 ml of mammosphere medium was added to each well. Mammosphere cultures were kept for 7 to 10 days at 37°C before using them for experiments. For the generation of acini, 50,000 isolated cells were seeded on a layer of growth factor-reduced Matrigel (Corning #344230) in assay medium with 2% of Matrigel (Corning #356231). Assay medium [DMEM/F12 (Gibco #11320-082), 2% Horse Serum (Invitrogen #16050-122), 0.5 μg/ml Hydrocortisone (Sigma-Aldrich #H-0888), 100 ng/ml Cholera Toxin (Sigma-Aldrich #C-8052), 10 μg/ml Insulin (ThermoFisher #12585-014), 1:100 Pen/Strep (Invitrogen #15070-06)] was supplemented with 5 ng/ml EGF (Peprotech #AF- 100-15-A) immediately before seeding cells. For generation of organoids, 100,000 freshly isolated mammary epithelial cells were seeded in a six- well low attachment plate in 2 mL per well of organoid media [DMEM/F12 (Gibco #11320-082), 5% Fetal Bovine Serum (Gibco #10438-026), 20 ng/ml bFGF (R&D Systems #233-FB-10), 10 ng/ml EGF (Peprotech #AF-100-15-A), 2.5 μM Rock inhibitor (EMD Millipore #420220), 4 ug/ml Heparin (Sigma-Aldrich #H3393)] with 3% Matrigel. After every 3-4 days 0.5 ml fresh media with Matrigel was added until used for experimental purposes. Cells were passaged for up to 15 times. Mammary epithelial cells from 11 weeks old bitransgenic MMTV-rtTA/TetO-NeuNT females (that never received doxycycline (DOX) while alive) were freshly isolated, grown in organoid media and induced *in vitro* with DOX for 48 h.

Treatment of acini and mammosphere cultures:

After 5-7 days in culture, acini were transfected with siRNA against mouse NR2F1 gene (Sigma Aldrich #SASI_Mm01_00118737 and #SASI_Mm_00118738), siRNA against human *Nr2f1* gene (Sigma Aldrich #SASI_Hs01_00095428), control siRNA (Thermo Fisher #AM4611), mouse *Mapk14* gene (Sigma Aldrich #SASI_Mm01_00020743), mouse *Mapk11* gene (Sigma Aldrich # SASI_Mm01_00044863). Acini were also transduced with shRNA against mouse *Nr2f1* gene (Origene #TL516691C and #TL516691D), or controlshRNA (Origene #TR30021, non-effective scrambled shRNA). Acini were fixed 48 h after transfection/transduction with 4%PFA and immunofluorescence assays were performed using the indicated antibodies. To measure mRNA changes, acini were transfected with the indicated siRNA and 48h later RNA was extracted from cultures using 1mL Trizol (Invitrogen #15596018) followed by RNA extraction. In some cases, cultures were treated for 24 hours with 1μM Lapatinib (SelleckChem #S2111), 200 ng/ml Wnt4 (R&D #475-WN-005/CF), 5μM SB203580 (Selleck #S1076), 2μM GSK2830371 (Selleck #S7573) or vehicle and RNA was extracted. In some cases, mammospheres growing in suspension conditions were transfected with siRNA against *Nr2f1* or control for 48h and then RNA was extracted. For evaluation of invasion in response to NR2F1 expression, ECCs were transduced with lentiviral particles carrying an NR2F1 responsive promoter driving RFP expression. The lentiviral vector used, (pLV[Exp]-Puro-COUP-TF cis

element>mRFP1), was custom-designed by VectorBuilder (vector ID: VB170830- 1011esp) and packaged in-house. Transduced cells were maintained in organoid cultures for up to 15 passages. Transduced acini were evaluated by Confocal Microscopy using a Leica SP5 confocal microscope and the LAS X Leica imaging software. For generation of stably MMTV-HER2 ECCs with NR2F1 depletion, freshly isolated MMTV-HER2 ECCs grown as mammospheres for 7 days were seeded in 2D and transduced with sh*Nr2f1* (Catalog #TL516691D) or shControl (Catalog #TR30021, non-effective scrambled shRNA). Transduced cells were selected with 1 μg/ml puromycin (Alpha Aesar #J67236) for 3 days. Then, stable MMTV-HER2 ECCs were cultured in organoid media, in presence of puromycin for the first week, and then for not more than 15 passages to avoid changes in phenotype and cellular properties. For mammosphere formation assays, stable shControl and sh*Nr2f1* MMTV-HER2 ECCs grown in organoids were seeded as single cells in 96 well plates and the number of spheres per well were quantified over time.

Migration assays.

MMTV-HER2 ECCs grown as organoids were transiently transfected with 1ug of pcDNA or mouse *Nr2f1*-ORF plasmids[13]. Then, 100,000 cells were seeded into the receiving chamber of transwell inserts with 8um pores (Corning #353097) in 200uL of serum-free medium. On the bottom chamber, in 24 well plates, 500uL of complete medium were added to establish a chemoattractant gradient. After 16 h, cells on the receiving chambers (non-migrated) were removed with a cotton swab. Migrated cells (on the opposite side of the membrane) were fixed with 4% PFA, stained with DAPI and the number of cells in ten random 20X fields were counted using inverted fluorescent microscope. Technical triplicates were included in all experiments.

Live Cell microscopy.

3D acini cultures were time-lapse imaged using an inverted microscope Olympus IX-70 with Live Cell enclosed chamber. We recorded 4 positions per condition in parallel for 2 hours with 10 minutes interval. Temperature was maintained at 37°C and CO2 at 5% throughout the imaging session. Movies were made by using either Metamorph® (Molecular Devices) or the open source imaging software ImageJ (RRID:SCR_003070)[18]. This was done using the services of the Microscopy CoRE at Icahn School of Medicine at Mount Sinai. This research was supported in part by the Tisch Cancer Institute at Mount Sinai P30 CA196521 – Cancer Center Support Grant. Protrusion number and their L/W ratio were quantified. In L/W ratio plots, data points represent the mean±SD of measurements taken by 2 independent operators. Invasive phenotype (a single elongated cell or cell file columns invading the Matrigel) or non- invasive phenotype was determined.

In vivo experiments.

Single cell suspension from organoids or mammosphere cultures were spun down at 230g for 4min and then 100,000 cells were suspended in 150μl PBS with 1mM calcium and 0.5mM magnesium (PBS++). Matrigel was then added in a 1:1 ratio. Cells were injected into one inguinal (#4) mammary gland fat pad using a 27-gauge needle. Injection sites were monitored for development of tumors weekly for 2 months and final tumor incidence was

calculated. Mice injected with PT derived cells were sacrificed when tumors reached 500 mm^3 according to IACUC regulations.

For 2-photon intra-vital microscopy of mammary glands, GFP-tagged stable MMTV-HER2 ECCs expressing either shControl or shNR2F1 lentiviruses were orthotopically injected in FOXN1^{nu} athymic mice (Jackson Laboratory). Mice were anesthetized using ketamine/xylazine and a skin flap surgery performed exposing the 4th and 5th mammary glands as previously described[19]. Intravital imaging was performed using an Olympus FV1000 MPE two-laser multiphoton microscope. An Infra-red tunable laser was used at 880nm excitation for imaging of GFP tagged cells. Imaging was done with a 25x 1.05NA (XLPL25XWMP2, Olympus) water immersion objective. For each mouse, fields were imaged at 5μm z steps to a depth of ~50μm, with each stack taken approximately every 2 min for 1 hour. Average number of movies per animal=2.2 to 3.8. Images were reconstructed and analyzed in ImageJ[18] utilizing the custom written ImageJ plugin ROI_Tracker[20]. Any residual x-y drift not eliminated by the fixturing window was removed with post processing using the StackReg plugin (https://doi.org/10.1109/83.650848) for ImageJ. All procedures were conducted in accordance with the National Institutes of Health regulations and approved by the Icahn School of Medicine at Mount Sinai animal use committee. Multiphoton microscopy was performed in the Microscopy CoRE at the Icahn School of Medicine at Mount Sinai, supported with funding from NIH Shared Instrumentation Grant (1S10RR026639).

Immunofluorescence (IF).

Three-Dimensional cultures were fixed with 4% PFA for 20min at room temperature. Staining was performed as previously described for MMTV-HER2 3D cultures[7]. Briefly, cells were permeabilized using 0.1% Triton X-100 for 20min and blocked using 1x IF wash buffer (components) + 10% Normal Goat Serum (Gibco, #PCN5000) for one hour. Primary antibodies were all used at 1:100 concentration unless specified otherwise. Antibodies used were: E-cadherin (BD Biosciences #610181; RRID:AB_397580); beta-catenin (BD biosciences 610153; RRID:AB_397554); Laminin V (Progen #10765; RRID:AB_2909803); CK14 (Biolegend #905301; RRID:AB_2565048); 1:25 NR2F1 (Abcam #ab181137; RRID:AB_2890250); PRRX1 (Novus Biologicals #NBP2-13816; RRID:AB_2909804); TWIST (Sigma-Aldrich#ABD29; RRID:AB_10807559); 1:50 HER2 (R&D #OP15L; RRID:AB_2099415); PH3 (Cell Signaling #9701S; RRID:AB_331535); SNAIL (Novus#NBP1-80022; RRID:AB_11039370); CK18 (Progen #GP-CK-18; RRID:AB_2909805); PanCK (eBioscience #42-9003-80; RRID:AB_10804753); Vimentin (R&D Systems #MAB2105; RRID:AB_2241653). The following secondary antibodies were used at 1:1000 dilution: Alexa fluor-488 goat anti-mouse (Invitrogen #A-11001; RRID:AB_2534069) and Alexa fluor-568 goat anti-rabbit (Invitrogen #A-11036; RRID:AB_10563566). F-Actin was detected using Alexa Fluor 568 Phalloidin (Invitrogen #A-12380). Chambers were removed from slides and wells were fixed and mounted with ProLong™ Gold Antifade reagent with DAPI (Invitrogen #P36931). Acini were imaged in 3D using a Leica SP5 confocal microscope and the LAS X Leica imaging software. Acini stained with anti-SNAIL antibody was considered positive when containing more than 3 z-stacks with more than 1 cell positive for nuclear SNAIL each. Acini stained with

anti-VIMENTIN antibody is considered positive when containing more than 3 z-stacks with one cell positive. Acini stained with anti-Ecadherin antibody is considered positive when containing more than 3 z-stacks with more than 3 positive cells each. Acini stained with anti- β-catenin antibody is considered positive when containing more than 5 positive cells with β-catenin localized in the membrane. For all experiments in acini cultures, MMTV-HER2 ECCs from 2 to 9 animal donors were used, and acini quantified ranged from 10-58 siControl (average=30) and 15-52 siNR2F1 (average=28) and data expressed per acinus or percentage of acini per condition. For experiments in acini cultures derived from organoids, at least two independent experiments were carried out, with 48 acini quantified by RFP expression.

Mammary gland section imaging was done using Leica DMi8 fluorescence microscope using LAS X Leica software. For IF staining of paraffin-embedded tissue: sections were routinely deparaffinized and rehydrated. Antigen retrieval was done in 10mM Sodium Citrate Buffer (pH 6) to later permeabilize using 0.1% Triton x-100 in PBS. Blocking was done using 3% BSA in PBS with 1.5% Normal Goat Serum or Normal Donkey Serum (Sigma-Aldrich #D9663; RRID:AB_2810235). Primary antibodies at 1:100 dilution unless otherwise specified – were assessed overnight at 4°C and secondary antibodies at 1:1000 dilution were assessed for one hour at room temperature. The following primary antibodies were used: beta-catenin (Cell Signaling #8480S; RRID:AB_11127855 or BD biosciences #610153, RRID:AB_397554); CK14 (Biolegend #905301; RRID:AB_2565048); 1:50 HER2 (Abcam, #ab2428; RRID:AB_303063 or R&D Systems #OP15L; RRID:AB_2099415); PH3 (Cell Signaling #9701S; RRID:AB_331535); TWIST1 (EMD Millipore # ABD29; RRID:AB_10807559); 1:25 NR2F1 (Abcam #ab181137; RRID:AB_2890250). The following secondary antibodies were used: Alexa Fluor-488 goat anti-mouse, Alexa Fluor-568 goat anti- rabbit, Alexa fluor-488 donkey anti-goat, Alexa fluor-647 donkey anti-rabbit (Invitrogen #A-31573; RRID:AB_2536183). Slides were mounted using Prolong™ Gold Antifade mounting media with DAPI (Molecular Probes #P36931).

Image Analysis.

All image analysis was performed in ImageJ. Circularity was calculated as Circularity=4pi(area/perimeter^2, with value of 1.0 indicating a perfect circle.

Flow Cytometry (FC).

For sorting of luminal cells, freshly isolated MMTV-HER2-CFP ECCs in single cell suspension were incubated for 30 min on ice with anti-mouse Fc Block CD16/32 antibody (Biolegend #101319; RRID:AB_1574973) in FACS buffer (1% BSA 2mM EDTA in PBS) to avoid non-specific antibody binding. Cells were then washed in FACS buffer and stained with fluorophore conjugated antibodies in FACS buffer. Cells were then washed in PBS and stained with Zombie NIR (Biolegend #423105) for 30 min on ice to determine live and dead (L/D) cell populations. Cell sorting of luminal ($Lin^{-}CD24^{HI}CD29^{+}$) cells was done over the live single cell population on an IMIL3 Sorter (BD Biosciences) from the Flow Cytometry Core at Mount Sinai School of Medicine. Antibodies used were: anti-CD45-PE (Miltenyi #130-117-498; RRID:AB_2727965); CD31-

PE (Miltenyi #130-119-653; RRID:AB_2751780); CD140a-PE (Miltenyi#130-102-502; RRID:AB_2660635); CD24-VioBlue (Miltenyi #130-102-734; RRID:AB_2656579); CD29-PE-Vio®770 (Miltenyi #130-105-125; RRID:AB_2660697). Cells were collected and seeded as described before for acinar cultures. For flow cytometry analysis after knockdown of NR2F1, acini cultured in Matrigel were collected in 2mM EDTA in PBS and incubated at 4 C for 1 h. Acini in suspension were trypsinized for 5 min and single cell suspension immediately processed for viability staining with Zombie NIR. Cells were then fixed in 4% paraformaldehyde and permeabilized using Perm/Wash buffer (BD #554723; RRID:AB_2869011). Antibodies used were: Cytokeratin 5-PE (Biorbyt #orb498435; RRID:AB_2909799); cytokeratin 14-CF640 (Biotium#BNC400532; RRID:AB_2909800); cytokeratin 18-CF488A (Biotium#BNC880041; RRID:AB_2909801); and cytokeratin 18-CF488A (Biotium#BNC880799; RRID:AB_2909802). Cells were then incubated with fluorescently labeled antibodies for intracellular detection of antigens. Cells were analyzed using an LSR Analyzer (BD) from the Flow Cytometry Core at Mount Sinai School of Medicine. Cells were gated in the following order: FSC/SSC> FCS-W/FSC-A>SSC-W/SSC-A> Lin-(CD45, CD31 and CD140a) > L/D (Zombie NIR−) > CFP+ > CD29/CD24 plots. Luminal cells sorted were cultured in matrigel to form acini and transfected with siRNAs as described previously at day 7 in culture and collected 48 h after. Knockdown validation for NR2F1 was done by IF and quantification of the MFI in the nuclear area (as RNA collected was limited by low cell number availability). Cell analyzed= 212 for siControl; 311 for siNR2F1.

Western Blot.

Samples were collected in RIPA buffer and centrifuged at 4°C, 18,000 g to clarify lysate. Protein concentration was determined by Pierce™ BCA Protein Assay Kit (Thermo Scientific #23225) and a standard BSA curve. Samples were then boiled for 5 min at 95°C in sample buffer (0.04M Tris-HCL pH 6.8, 1%SDS, 1% β-mercaptoethanol and 10% glycerol). SDS- PAGE 10% gels were run in Running Buffer (25mM Tris, 190mM glycine, 0.1% SDS) and transferred to PVDF membranes in Transfer Buffer (25mM Tris base, 190mM glycine, 20% methanol). Membranes were then blocked in 5% milk in TBST. Primary antibodies were left overnight at 4°C. Following washing with TBST buffer HRP conjugated secondary antibodies were left at room temperature for one hour. Western blot development was done using Amersham ECL Western Blot Detection (GE #RPN 2106) and GE ImageQuant LAS 4010. Primary antibodies used were: p38 1:500 (Cell Signaling #9212; RRID:AB_330713); p-p38 (Thr180/Tyr182) 1:1000 (Cell Signaling #4511; RRID:AB_2139682), p38alpha 1:5000 (BD # 612168; RRID:AB_399539), GAPDH 1:1000 (Cell Signaling #5174; RRID:AB_10622025); NR2F1 1:500: (Abcam #ab181137; RRID:AB_2890250), pS6 1:1000 (Cell Signaling #5364; RRID:AB_10694233), Tubulin 1:1000 (abcam #15568; RRID:AB_2210952), Total b-Catenin 1:1000 (Cell Signaling #8480; RRID:AB_11127855), Lamin B1 1:1000 (Cell Signaling #12586; RRID:AB_2650517), ATF2 1:1000 (Cell Signaling #35031; RRID:AB_2799069), p-ATF2/ATF7 1:1000 (Cell Signaling #24329; RRID:AB_2909807), p-HER2/ErbB2 1:1000 (Cell Signaling #2243; RRID:AB_490899). Secondary antibodies used were Peroxidase Horse Anti-Mouse IgG (1:5000) (Vector #PI-2000; RRID:AB_2336177) or anti-rabbit IgG (1:5000) ((Vector #PI-1000; RRID:AB_2336198).

QPCR.

RNA was extracted from 2D or 3D cell cultures using Trizol following provider's recommendation. For early mammary gland tissue RNA was extracted using Qiagen's RNeasy Lipid Tissue Midi Kit (Qiagen #74804). RNA (1-2 μg) was retrotranscribed into cDNA using RevertAid First Strand cDNA Synthesis Kit (Thermo Scientific # K1621). Quantitative real time-PCR was performed using PerfeCTa SYBR green (Quantabio, #P/N 84069) in Biorad thermocycler. *Gapdh* was used as reference gene control for all plates. All reactions were carried out with technical triplicates. Mouse Q-PCR primers were: *Gapdh* forward primer 5'-AACTTTGGCATTGTGGAAGGGCTC-3'; *Gapdh* reverse primer 5'-TGGAAGAGTGGGAGTTGCTGTTGA-3'; *Twist1* forward primer 5'-AACTGGCCTGCAAAATCATA −3'; *Twist1* reverse primer 5'-ACACCGGATCTATTTGCATT-3'; *Zeb1* forward primer 5-ACCCCTTCAAGAACCGCTTT-3'; *Zeb1* reverse primer 5- CAATTGGCCACCACTGCTAA-3'; *Nr2f1* forward primer 5'-CCAATACTGCCGCCTCAA-3'; *Nr2f1* reverse primer 5'-GGTTGGAGGCATTCTTCCTC-3'; *Prrx1* forward primer 5'-GCACAAGCAGACGAAAGTGT-3'; *Prrx1* reverse primer 5'-CTGGTCATTGTCCTGCTGAG-3'; *Snai1* forward primer 5'-GGCGGAAGCCCAACTATAGC-3', *Snai1* reverse primer 5'-AGGGCTGCTGGAAGGTGAA-3'; *Vim* forward primer 5'-AGGAGGCCGAAAGCACCCTGC-3', *Vim* reverse primer 5'-CCGTTCAAGGTCAAGACGTGCCA-3'; *Cdh1* forward primer 5'-ACAGACCCCACGACCAATGA-3', *Cdh1* reverse primer 5'-CCTCGTTCTCCACTCTCACA-3'; *Axin2* forward primer 5'-CAAAAGCCACCCAAAGGCTC -3', *Axin2* reverse primer 5'-TGCATTCCGTTTTGGCAAGG-3', P38alpha (*Mapk14*) forward primer 5'-TGACCCTTATGACCAGTCCTTT-3'; P38alpha (*Mapk14*) reverse primer 5'-GTCAGGCTCTTCCACTCATCTAT-3'; P38beta (*Mapk11*) forward primer 5'-GCGGGATTCTACCGGCAAG-3'; P38beta (*Mapk11*) reverse primer 5'-GAGCAGACTGAGCCGTAGG-3'. Human QPCR primers were: *PRRX1* forward primer 5'-CTGATGCTTTTGTGCGAGAA-3'; *PRRX1* reverse primer 5'-ACTTGGCTCTTCGGTTCTGA-3'; *ZEB1* forward primer 5'-GATGATGAATGCGAGTCAGATGC-3'; *ZEB1* reverse primer 5'-ACAGCAGTGTCTTGTTGTTGT-3'; *TWIST1* forward primer 5'-TGCAGCTATGTGGCTCACGA-3'; TWIST1 reverse primer 5'-ACAATGACATCTAGGTCTCCGGC-3'; *CDH1* forward primer 5'-CGAGAGCTACACGTTCACGG-3'; *CDH1* reverse primer 5'-GGGTGTCGAGGGAAAAATAGG-3'. Rat HER2 expression in the MMTV-rtTA-TetO-Neu cells was determined by Taqman assays against rat Her2 (Rn00566561_m1-FAM; Thermo Fisher) for rat Erbb2 and Gapdh (Mm99999915_g1-FAM); Thermo Fisher) and expressed as fold change over unspecific levels from unstimulated samples.

Patient samples.

Paraffin embedded sections from DCIS and invasive breast cancer patient tumors were obtained from the Cancer Biorepository at Icahn School of Medicine at Mount Sinai,

New York, NY. Samples were de-identified and obtained with Institutional Review Board approval, which indicated that this work does not meet the definition of human subject research according to the 45 CFR 46 and the Office of Human Subject Research. IF and immunohistochemistry (IHC) analysis was done using samples from 21 DCIS patients. Benign adjacent (BA) and tumor areas from DCIS patients were identified by a pathologist in adjacent sections stained with H&E. Paraffin embedded sections from DCIS patient samples injected in animals (MIND model [21]) were obtained from Dr. Behbod. Samples were de-identified and obtained with Institutional Review Board approval. The arbitrary threshold for NR2F1 levels (negative, high and low) was established by comparing distribution plots of the MFI for NR2F1 and IgG for all benign tissues and DCIS samples. We followed a similar approach using distribution plots of the MFI for PRRX1 and IgG in all samples to establish PRRX1 levels (negative, high and low). $NR2F1^{LOW}/PRRX1^{HIGH}$ ratio was determined over HER2− (n=6) and HER2+ (n=7) DCIS samples (including DCIS sections from mouse mammary intraductal (MIND) model [21]), and benign adjacent tissues (n=6). MFI values were quantified from the DAPI+ (nuclear) areas of all panCK+ cells per FOV (>8,000 cells). Percentage of cells with $NR2F1^{LOW}/PRRX1^{HIGH}$ staining was calculated per samples and the frequency of samples positive and negative for this staining was determined per group and plotted (right panel).

Immunohistochemistry and HER2 scoring.

Sections were routinely deparaffinized and rehydrated before staining procedures. Sections were treated with stabilized 3 % hydrogen peroxide solution for 30 min to block endogenous peroxidase activity, incubated in a water bath immersed in sodium citrate buffer (pH 6.0) for 40 min at 97 °C for antigen retrieval, and incubated with 3 % BSA in PBS for 1 hour to block nonspecific binding, washing thoroughly in PBS between steps. HER2 immunohistochemistry was performed with Anti-c-ErbB2/c-Neu (Ab-3) Mouse mAb (3B5) 1/200 (Sigma-Aldrich t# OP15) overnight at 4°C. After washing, secondary Horse Anti-Mouse IgG Antibody (H+L), Peroxidase (Vector# PI-2000) was added diluted 1/200 for 1 h at room temperature. Signal was developed for 10 min in DAB solution (Vector #SK-4100 prepared according to manufacturer instructions), sections were then counterstained for 1 min with Harris hematoxylin, rehydrated, and mounted. Negative controls using mouse IgG showed no immunoreactivity. Evaluation of immunostainings was performed by a trained pathologist and scored according to ASCO/CAP guidelines[22]: negative for 0 (no membrane staining) and 1+ (faint or barely perceptible incomplete membrane staining); equivocal for 2+ (moderate circumferential staining in >10% of tumor cells or strong circumferential membranous staining in ≤10% of tumor cells) and positive for 3+ (strong circumferential membranous staining in >10% of tumor cells).

NR2F1 immunohystochemistry was performed with 1:100 NR2F1 (Abcam #ab41858) following the same protocol. Total nuclear NR2F1 was detected and quantified.

Statistical Analysis.

Statistical Analysis was done using Prism Software (RRID:SCR_002798). Differences were considered significant if P values were <0.05. For the majority of *in vitro* experiments, two-tailed Student's t-test was performed unless otherwise specified. For mouse experiments

and human samples two-tailed Mann-Whitney test was used. Sample size chosen was done empirically. To determine the frequency of samples carrying $NR2F1^{LOW}/PRRX1^{HIGH}$ ratio between benign adjacent and DCIS samples, Fisher's exact test was used. Research reported in this publication was supported in part by the National Cancer Institute Cancer Center Support Grant P30CA196521-07 awarded to the Tisch Cancer Institute of the Icahn School of Medicine at Mount Sinai and used the Biostatistics Shared Resource Facility. The content is solely the responsibility of the authors and does not necessarily represent the official views of the National Institutes of Health.

Data were generated by the authors and included in the article.

RESULTS

NR2F1 expression is positively regulated by MAPK-p38 signaling downstream of HER2 in early breast cancer cells.

Previous studies have shown that p38α/β signaling was enriched in a dormancy model of HNSCC cells and positively regulated NR2F1 levels [13, 14]. As the phosphorylation of both p38α and p38β isoforms and NR2F1 expression (mRNA and protein) were reduced in early lesions of MMTV-HER2 mice when compared to normal mammary glands from FvB female siblings [7, 13, 23], we aimed to determine whether downregulation of NR2F1 in HER2+ ECCs was functionally linked to a reduction in p38 α/β activity. To this end, we treated young MMTV-HER2 females with a p38α/β inhibitor (SB203580), a time when this kinase is active in the mammary epithelium[7]. p38α/β inhibition further downregulated *Nr2f1* mRNA and protein levels in mammary glands when compared to vehicle group (Fig. 1A). *In vitro*, p38α/β inhibition did not change the levels of *Nr2f2*, another member of the NR2F-family, although suppression of E-cadherin and induction of TWIST1 (twist basic helix-loop-helix transcription factor 1) expression was observed, as reported[7] (Supp. Fig. 1A). Wang et. al.,[24] have recently showed that inhibition of the wild-type p53 induced phosphatase (WIP1) increased p-p38 levels in MMTV-HER2 ECCs and reduced dissemination of ECCs [24]. We therefore determined whether treatment of MMTV-HER2 ECCs with WIP1 inhibitor (GSK2830371) could modulate *Nr2f1* levels. We observed increased levels of p-p38 and *Nr2f1* (Supp. Fig. 1B), but no changes in the levels of *Nr2f2* (Supp. Fig. 1B). We also analyzed the regulation of NR2F1 by p38 in the genetically advanced MDA-MD-361 and BT474 HER2+ tumor cell lines and again observed upregulation of p-p38 levels upon treatment with WIP1 inhibitor in the absence of changes in NR2F1 or *Nr2f2* expression (Supp. Fig. 1C). These results support the idea that context-specific regulation occurs at different stages of HER2-driven breast tumor progression. Moreover, $MKK3^{-/-}/MKK6^{+/-}$ (mitogen-activated protein kinase kinase 3/6) mice, with targeted disruptions of the *Map2k3* and *Map2k6* genes, both of which are upstream activators of p38, also showed reduced NR2F1 protein levels compared to syngeneic wild-type (WT) mice (Sup. Fig. 1D), supporting the idea that even in the normal mammary gland, MKK3/6-p38α/β signaling regulates expression of NR2F1. To determine which p38α or p38β isoforms regulated NR2F1 expression in MMTV-HER2 ECCs, we used siRNAs directed against *Mapk14* (p38α) and *Mapk11* (p38β) isoforms and measured NR2F1 levels. While we observed downregulation of NR2F1 in cells transfected with

sip38α but not sip38β (Supp. Fig. 1E&F), in contrast, *Nr2f2* was not regulated by either p38 isoform (Supp. Fig. 1E&F). Together, these results suggest that p38α regulates NR2F1 expression but not *Nr2f2* in MMTV-HER2 ECCs.

Next, we decided to determine whether HER2 negatively regulated NR2F1 in ECCs. First, we evaluated whether HER2+ ECCs had low levels of NR2F1 expression using immunofluorescence (IF) staining. Our results showed that approximately 90% of HER2+ mammary cells expressed low/negative levels (based on fluorescence intensity threshold) of NR2F1 (Fig. 1B). Inhibition of HER2 (and HER1) with lapatinib upregulated *Nr2f1* levels in MMTV-HER2 ECCs (Fig. 1C) but not in normal FvB mammary epithelial cells (Supp. Fig. 1G). Moreover, addition of doxycycline (DOX) to mammary epithelial cell cultures isolated from unstimulated MMTV-rtTA/TetO-Neu (HER2 inducible) females induced *Erbb2* rat oncogene expression and caused downregulation of *Nr2f1* when compared to vehicle-treated controls (Fig. 1D). *Nr2f1* levels were also upregulated in lapatinib-treated human HER2+ SUM225 DCIS cells originally established from a DCIS patient [25] when compared to control cells (Supp. Fig. 1H). However, we did not observe changes in *NR2F1* or *NR2F2* levels after depletion of HER2 oncogene in genetically advanced human HER2+ tumor cell lines (Supp. Fig. 1I), supporting our previous data (Supp. Fig. 1C) which demonstrated that genetically evolved MDA-MD-361 and BT474 cells do not share the same upstream signaling pathway that controls *Nr2f1* expression.

To determine whether HER2 was inhibiting *Nr2f1* expression via p38, we treated MMTV-HER2 ECCs with SB203580 and TAK-715, a p38 inhibitor that is 28-fold more selective for p38α than p38β and does not inhibit p38γ/δ[26], in presence or absence of lapatinib (Fig. 1E). Lapatinib-induced *Nr2f1* re-expression was blocked in the presence of SB203580 or TAK-715 (Fig. 1E, Supp. Fig. 1J). Similar results were obtained in human HER2+ SUM225 DCIS cells (Supp. Fig. 1K). Overall, these studies suggest that HER2 blocks NR2F1 expression via p38 signaling in human and murine pre-malignant models.

We showed that WNT4 was a member of a progesterone-driven signature that mediated dissemination of ECCs [6]. Importantly, we observed downregulation of NR2F1 expression upon treatment of ECCs with WNT4 (Fig. 1F&G). We conclude that the activation of HER2 and WNT4 signaling causes reduced expression of NR2F1 in HER2+ ECCs.

We next examined the expression of NR2F1 in human DCIS using IF and observed significant reduction in the percentage of nuclear NR2F1 positive cells in DCIS when compared to benign adjacent lesions (Fig. 1H, Supp. Fig. 2A-C). We then correlated NR2F1 levels in DCIS with HER2 status (Supp. Fig. 2) and observed that the percentage of NR2F1 negative cells and the percentage of $NR2F1^{HIGH}$ cells remarkably increased and decreased, respectively in HER2+ DCIS samples ($p<0.0001$) when compared to benign adjacent lesions (Fig. 1I, Supp. Fig. 2A-C). It is, however, interesting that HER2− DCIS samples were also mostly low/negative for NR2F1 expression when compared to benign adjacent lesions ($p<0.0001$ for NR2F1 negative population; $p<0.01$ for $NR2F1^{LOW}$ population) (Fig. 1I, Supp. Fig. 2A-C). This was not altogether surprising as other oncogenic signals such as MYC have been reported to reduce NR2F1 protein levels in early lessions from MMTV-Myc females [13]. These results suggest that alternative mechanisms, such as MYC oncogene or

progesterone-induced paracrine signals as shown in Fig. 1F&G, could be involved in NR2F1 downregulation and that the loss of NR2F1 is by itself a crucial step in the early steps of cancer progression.

NR2F1 downregulation favors a motile phenotype and *in vivo* invasion in early breast cancer cells.

NR2F1 has been linked to growth suppression, lineage commitment and differentiation [13, 27, 28]. However, some studies have shown a role in promoting cell migration and axogenesis [29, 30]. Further, because reduced p38α/β signaling in HER2+ ECCs caused accelerated early dissemination [7, 24], and our data (Fig. 1A&E and Supp. Fig. 1B, D, E, J,&K) showed that p38 regulated NR2F1, we hypothesized that low NR2F1 levels will correlate with an invasive phenotype in MMTV-HER2 ECCs. To test this, MMTV-HER2 ECC acini were transduced with a lentiviral vector carrying an RFP-reporter for NR2F1 activity and quantified by confocal microscopy. The results showed that ~70% of ECCs that invaded outwards from the acini had low NR2F1 activity (Fig. 2A) while we observed consistently intra-acinar NR2F1-reporter activity.

Next, we used time-lapse microscopy to track and quantify cell dissemination into 3D Matrigel using siRNA and shRNA against *Nr2f1* in MMTV-HER2 ECCs acini. NR2F1 depletion was efficient at the protein and mRNA levels (Supp. Fig. 3A-D), did not change *Nr2f2* levels (Supp. Fig. 3D) and did not induce apoptosis (Supp. Fig. 3E). The results of this study showed that while individual cells moving on the surface of siControl acini largely remain rounded, NR2F1 downregulation induced cell file columns invading the Matrigel (Fig. 2B-D, Movies 1-4). Analysis of the length-over-width ratio of the protrusions (one cell or cell file columns) showed higher elongation towards the Matrigel in the siNR2F1 group when compared to control group (Fig. 2B&2E, Supp. Fig. 3F&G). The number of protrusions per acini did not change between siControl *vs.* si*Nr2f1* group (Supp. Fig. 3H). However, we observed higher percentage of protrusions with an invasive phenotype (a single elongated cell or cell file columns invading the Matrigel) after *Nr2f1* knockdown compared to the control group (Fig. 2C, D & F, Supp. Fig. 3I). Moreover, overexpression of *Nr2f1* (Supp. Fig. 3J) in MMTV-HER2 ECCs significantly decreased their migratory capacity, as shown by migration assay in transwell® inserts (Fig. 2G).

Next, we quantified how downregulation of NR2F1 expression affects the invasion *in vivo*. We performed intravital imaging through mammary fat pad windows [19] (Fig. 2H) of GFP-tagged MMTV-HER2 ECCs stably expressing either shControl or shRNA targeting *Nr2f1* (Supp. Fig. 3K). Intravital time-lapse imaging revealed that GFP positive cells were viable and organized in acinar-like structures (representing ~60%) or duct-like structures (~40%) at the same proportions in shControl *vs.* sh*Nr2f1* injected ECCs (Supp. Fig. 3L). Two-photon microscopy analysis showed that NR2F1 downregulation significantly increased the dissemination of ECCs from acini into the surrounding stroma when compared to shControl ECCs (Fig. 2I&J, Movies 5, 6). Analysis of the acini morphology showed less circularity and fewer cells per area in sh*Nr2f1* acini than shControl acini, suggesting increased motility (Supp. Fig. 3M).

To reinforce the link between HER2 and NR2F1 in ECCs, we tested the effect of lapatinib in ECCs that had lost NR2F1 expression using intravital imaging. Mice injected with shControl or sh*Nr2f1* MMTV-HER2 ECCs were treated with either DMSO or lapatinib for 48 hours followed by intravital imaging through mammary fat pad windows. The efficacy of lapatinib was verified by *in situ* staining of mammary gland plugs with a pS6 (ribosomal protein S6) antibody (Supp. Fig. 3N). Treatment with lapatinib inhibited invasion of ECCs isolated from mice injected with the control shRNA but not those injected with sh*Nr2f1*, arguing that lapatinib was not able to restore NR2F1 expression under these conditions (Fig. 2K). Percentage of cleaved-caspase 3 (CC3) positive ECCs in DMSO- and lapatinib-treated mice showed no differences (Supp. Fig. 3O). These results imply that the motility of HER2+ ECCs is NR2F1 dependent and that NR2F1 acts as a barrier for dissemination downstream of HER2.

NR2F1 blunts the expression of specific EMT regulators and establishes a hybrid luminal/basal phenotype in early breast cancer cells.

We previously reported that MMTV-HER2 ECCs gained expression of the EMT gene TWIST1 and reduced the expression of E-cadherin[7]. We hypothesized that if NR2F1 limits early dissemination, it might regulate components of the EMT program. In support of our hypothesis, we found that depletion of *Nr2f1* decreased E-cadherin levels and junctions in MMTV-HER2 ECCs acini and 2D at the mRNA and protein levels, suggesting destabilization (Fig. 3A&B, Supp. Fig. 4A). Furthermore, the EMT master regulators TWIST1, PRRX1 and *Zeb1* (zinc finger E-box binding homeobox 1) were upregulated in shNR2F1 MMTV-HER2 ECCs acini and *in situ* staining from mammary gland tissues when compared to shControl group (Fig. 3A, C&D, Supp. Fig. 4B, Supp. Fig. 3K). Depletion of *NR2F1* mRNA levels in HER2+ SUM225 DCIS cells decreased E-cadherin levels and upregulated *TWIST1* and *ZEB1* mRNA levels without affecting *NR2F2* levels (Supp. Fig. 4C). The mRNA levels of *PRRX1* were too low to be detected by qPCR in SUM225 cells. We also observed upregulation of *Zeb1* and *Prrx1* levels in SB203580-treated MMTV-HER2 ECCs acini when compared to DMSO-treated acini (Supp. Fig. 4D). *Nr2f1* knockdown reduced E-cadherin in FvB normal acini; however, it was not accompanied by transcriptional changes in the expression of EMT master regulators (Supp. Fig. 4E). These results suggest that these mechanisms are specific to oncogenic HER2-regulated early progression stages. The protein levels of SNAIL (snail family zinc finger 1) and VIMENTIN (the latter of which was very low) in MMTV-HER2 ECCs upon *Nr2f1* knockdown were not affected (Supp. Fig. 4F&G). These findings support the notion that only certain components of the EMT program are controlled by NR2F1.

To determine whether low levels of NR2F1 and high levels of EMT genes are inversely correlated, we stained benign adjacent tissues and DCIS samples using anti-NR2F1 and anti-PRRX1 antibodies (Fig. 3E, and see methods). We analyzed paraffin-embedded DCIS sections and sections from the MIND model, which where freshly isolated patient-derived DCIS cells were injected in athymic mice[31]. These studies revealed that the $NR2F1^{LOW}$/$PRRX1^{HIGH}$ ratio was more frequently detected in DCIS (HER2+ and HER2−) samples than in benign adjacent tissues (Fig. 3E).

Next, we investigated whether NR2F1 controls β-catenin localization as this Wnt-regulated signal was associated with early dissemination in our prior studies[7]. Immunofluorescence (IF) staining using a total β- catenin antibody showed less membranous localization in NR2F1-depleted MMTV-HER2 ECC acini and mammary glands than in controls (Fig. 3F, Supp. Fig. 4H), similar to what we had observed when p38 was inhibited[7]. Unfortunately, due to the limited sensitivity of the technique[7], IF detection of nuclear β-catenin was not possible. To address this issue, we transfected MMTV-HER2 ECC acini with either siControl or si*Nr2f1*#2 (which targets a different sequence in the *Nr2f1* gene than that used in previous experiments) and subjected nuclear fractions to western blot analysis. Increased accumulation of nuclear β-catenin after *Nr2f1* depletion was observed when compared with control cells (Supp. Fig. 4I), suggesting that disappearance of membrane β-catenin upon *Nr2f1* depletion correlates with β-catenin nuclear accumulation. To determine whether NR2F1 regulated β-catenin localization in a WNT-dependent manner, we transfected MMTV-HER2 ECC acini with either siControl or si*Nr2f1*#2 (Supp. Fig. 4J) and treated MMTV-HER2 ECC acini with either vehicle or DKK1, a WNT inhibitor. As expected, siNR2F1#2 decreased membrane localization of β-catenin localization when compared to siControl conditions (Fig. 3G), which is consistent with our previous studies (Fig. 3F and Supp. Fig. 4H). The addition of DKK1 did not affect membrane β-catenin localization in siControl ECC acini; however, it was able to block the decrease in membrane β-catenin localization upon NR2F1 depletion (Fig. 3G). This result suggests that NR2F1 blocks β-catenin nuclear localization downstream of WNT signaling. Moreover, unlike what we observed with p38 α/β inhibition, the mRNA levels of *Axin2*, a transcriptional target of Wnt/β-catenin that creates a negative feedback loop to silence the signaling pathway, did not increase upon NR2F1 knockdown (Supp. Fig. 4K). Overall, these results suggest that NR2F1 knockdown leads to translocation of nuclear β-catenin from the membrane to the nucleus via WNT-regulated pathways.

It has been previously shown that NR2F1 expression correlates with a more luminal phenotype in mammary epithelial cells[32] and acquisition of a basal phenotype has been linked to dissemination, metastasis and poor survival[33-35]. Our studies revealed that knockdown of *Nr2f1* resulted in an increase in the percentage of CK14+ invading cells in MMTV-HER2 ECCs acini (Fig. 3H) and 2D (Supp. Fig. 5A), which is consistent with increased levels of CK14 expression in acini-like structures measured after injection of shNR2F1 MMTV-HER2 ECCs into the fat pad of nude mice (Supp. Fig. 5B). Interestingly, depletion of NR2F1 in MMTV-HER2 ECC acini (Supp. Fig. 5C) did not change the percentages of CK5, CK18 or CK19 positive cells detected by flow cytometry (Fig. 3I) and slightly increased *Krt5* mRNA levels (Supp. Fig. 5D). Furthermore, NR2F1 downregulation slightly reduced *Gata3* (GATA binding protein 3) mRNA levels in MMTV-HER2 ECCs (Supp. Fig. 5D). Moreover, no changes in the percentages of viable sorted out luminal MMTV-HER2 ECCs or changes in the percentages of CK18 positive cells were observed as a function of NR2F1 expression (Supp. Fig. 5E-G), which is in agreement with the results from bulk primary cultures shown in Fig. 3I. These results suggest that NR2F1 depletion does not selectively induce luminal cell death and favors the acquisition of a hybrid luminal/basal phenotype in ECCs.

Lastly, we observed that NR2F1 depletion disrupted laminin 5 deposition in MMTV-HER2 ECCs acini (Fig. 3J), supporting that downregulation of NR2F1 allows ECCs to invade into interstitial space. This result was also observed when MMTV-HER2 ECCs acini were treated with the p38 inhibitor SB203580[7].

Based on these results we argue that depletion of NR2F1 in ECCs allows them to acquire a partial EMT program and a basal/luminal hybrid phenotype, which are required for early dissemination.

Loss of NR2F1 in the mammary epithelium favors early spontaneous dissemination to the lungs.

To assess the tumor-initiating ability of ECCs after NR2F1 knockdown, we injected either shControl or sh*Nr2f1* MMTV-HER2 ECCs (Supp. Fig. 3K) in the mammary fat pads of nude mice and monitored tumor outgrowth. Mice injected with shControl MMTV-HER2 ECCs did not develop tumors over the 2 month monitoring period (Fig. 4A), which is in agreement with our previous work showing that MMTV-HER2 ECCs are largely non-tumorigenic in orthotopic sites[7]. Interestingly, mice injected with sh*Nr2f1* MMTV-HER2 ECCs did not develop tumors (Fig. 4A). By contrast, we observed tumor take in all mice injected with late stage MMTV-HER2 tumor cells as previously shown[7] (Fig. 4A). sh*Nr2f1* MMTV-HER2 ECCs injected into the fat pad had the same percentage of cells that stained positive for the proliferative marker phospho-histone 3 (PH3) when compared to shControl cells (Fig. 4B). The same result was observed in MMTV-HER2 3D acini (Supp. Fig. 5H). These results suggest that downregulation of NR2F1 do not induce primary tumor outgrowth in animals. To assess the *in vitro* stemness capacity of MMTV-HER2 ECCs after *Nr2f1* knockdown, we transduced MMTV-HER2 ECCs with shControl or sh*Nr2f1* lentiviruses and measured number of mammospheres. We observed an increased number of spheres upon *Nr2f1* depletion when compared to shControl group (Supp. Fig. 5I), leading us to conclude that *Nr2f1* knockdown induces proliferation and stemness in *in vitro* mammospheres assays. However, in *in vivo* experiments, the dissemination of ECCs upon NR2F1 knockdown dominates over the proliferation capacity. We therefore did not observe tumor formation upon *Nr2f1* knockdown (Fig. 4A) and similar levels of PH3 positive cells were detected in shC and sh*Nr2f1* ECCs injected in the fat pad of nude mice (Fig. 4B).

To strengthen our hypothesis concerning the role of NR2F1 in spontaneous dissemination to the lungs, we harvested the lungs of the above-mentioned mice after a 10-16 day period post-injection to measure the number of infiltrating eDCCs (Fig. 4C&D). The number of single lung eDCCs was higher in sh*Nr2f1* group when compared to shControl group (Fig. 4D), supporting the notion that NR2F1 represses systemic dissemination to distant organs such as the lung. At this time point, there was no difference in the percentage of proliferative eDCCs measured by PH3 staining (Fig. 4E), which ruled out the possibility that the increased number of eDCCs seen in sh*Nr2f1* group was due to the capacity of eDCCs to start proliferating immediately. It is worth mentioning that no metastases were found in either group, as metastases take longer to develop due to a prolonged dormancy phase[7].

Overall, our results suggest that during early stages of cancer progression, NR2F1 primarily functions to limit an EMT- and a hybrid luminal/basal-like dissemination program activated

by HER2 signaling which is linked to motility and invasion processes rather than a “growth-limiting” program (Fig. 5).

DISCUSSION

Our study expands our understanding of how an early-established HER2-dependent program primarily deregulates motility and invasion to favor dissemination of HER2+ ECCs to secondary organs before activating oncogene addictive growth (Fig. 5).

We report that NR2F1 is positively regulated by p38α signaling and repressed by HER2 and WNT4 pathways in human and murine HER2+ ECCs but not in genetically evolved HER2+ tumor cell lines. Recent papers that built on our previous work on the HER2-p38 axis[7] have reported a HER2-dependent degradation of Tpl2 (mitogen-activated protein kinase kinase kinase 8) and that inhibition of Tpl2 enhanced early dissemination in the MMTV-HER2 mouse model [36]. Whether NR2F1 is transcriptionally or post-trancriptionally regulated by Tpl2 activity will be the focus of future work.

Supporting the idea of a linear signaling pathway that has p38α upstream of NR2F1 in HER2+ ECCs is the fact that a WIP1 inhibitor, which has been shown to increase p-p38 and E-cadherin levels and prevent early dissemination in the MMTV-HER2 mouse model[24] also increased NR2F1 expression (Supp. Fig. 1B). Moreover, NR2F1 blocked the expression of *Zeb1* and TWIST1, known negative regulators of E-cadherin[37, 38]. Genomic data analysis revealed two peaks for the NR2F1 binding in the *ZEB1* promoter in GM12878 cells (ENCSR514VYD data set, ENCODE). Moreover, Rada-Iglesias and et. al., showed the binding of NR2F1 to *Twist1* promoter using NR2F1 ChIP assays in neural crest cells [28]. Future work is needed to validate the binding of NR2F1 in ZEB1 and TWIST1 promoter regions in HER2+ ECCs by ChIP analysis. Here, we showed that NR2F1 blocked β-catenin nuclear localization downstream of WNT (Fig. 3G and Supp. Fig. 4I). Previous studies in MMTV-HER2 ECCs have reported that inhibition of MK2 (MAP kinase-activated protein kinase 2), a target of p38, led to decreased levels of phosphorylated HSP27, resulting in its ability to activate β-catenin[24]. Thus, future work will focus on understanding whether NR2F1 regulates HSP27 (heat shock protein 2) phosphorylation to induce β-catenin activity.

We also observed that NR2F1 depletion in ECCs increased PRRX1 expression. PRRX1 is particularly interesting, as PRRX1a and PRRX1b isoforms have been involved in tumor progression and they play important roles in metastatic outgrowth and dissemination, respectively[39]. Whether NR2F1 can modulate the alternative splicing of PRRX1 in the mammary epithelium remains to be elucidated.

Simultaneous overexpression of TWIST1 and downregulation of E-cadherin in normal mammary epithelial cells has been shown to increase cell motility in cells expressing the basal CK14 and luminal CK8 markers [40]. Our data shows the same hybrid luminal/basal phenotype acquired by pre-malignant lesions upon the depletion of NR2F1 that may facilitate dissemination, survival at ectopic sites, drug resistance and tumor-initiating potential[41].

NR2F1 regulates dormancy in a variety of tumor types[13]. NR2F1 expression is relatively low in breast, HNSCC and prostate primary tumors. However, once cancer cells disseminate to secondary organs as DCCs they regain NR2F1 expression[13, 42]. We also showed that NR2F1, downstream of p38 signaling, regulated dormancy of late DCCs in advanced tumor models[13] and that detection of NR2F1 in DCCs from breast and prostate cancer patient's bone marrow aspirates correlated with good prognosis[43, 44]. Moreover, we showed that the dormancy program of eDCCs was p38-independent[7]. These results indicate that different dormancy programs are present in early *vs.*. late DCCs. Whether NR2F1 expression is regained in eDCCs and whether it plays a role in dormancy of eDCCs remains to be determined.

The downregulation of NR2F1 levels was linked to the deletion of a susceptibility locus in a rat-human comparative genetic analysis[45]. Thus, determining these susceptibility loci may predict patients at risk for early spread, especially for those patients with family history. In this study, we have corroborated the detection of an inverse correlation between NR2F1 and PRRX1 expression in human HER2+ and HER2− DCIS samples. The clinical application of this result needs to be further evaluated by determining the association of $NR2F1^{LOW}/PRRX1^{HIGH}$ ratio with the clinical detection of eDCCs and whether it could be used to predict the risk of relapses in HER2+ and HER2− patients. Furthermore, our intravital imaging results suggest that treatment of patients carrying HER2+ pre-malignant lesions may benefit from lapatinib treatments if NR2F1 levels are able to be restored by lapatinib.

Supplementary Material

Refer to Web version on PubMed Central for supplementary material.

Acknowledgements

We thank Dr. Roger Davis for $MKK3^{-/-}/MKK6^{+/-}$ samples and his valuable feedback. We also thank Dr. Skobe for providing the BT474 and MDA-MB-361 cells.

Grant support:

CCR17483357 (M.S.S.); MRF-CDA (M.S.S); K22CA201054 (M.S.S); CSBC Pilot Project-Sage Bionetworks (M.S.S.); Schneider-Lesser Foundation Fellow Award (M.S.S); MRA (M.S.S); BCA (M.S.S.), CCR18547848 (J.J.B-C); R01CA244780 (J.J.B-C); K22CA196750 (J.J.B-C); P30-CA196521(J.J.B-C); NIH-R00 CA127462 (FB); NIH-R01CA207445 (FB); NIH-R21CA226567 (FB); P30 CA168524 (FB); P20 GM130423 (FB); UL1TR002366 (FB); C38317/A24043 (FB); P30CA196521-07 (ISMMS); 1S10RR026639 (ISMMS).

REFERENCES

1. Braun S, et al. , Cytokeratin-positive cells in the bone marrow and survival of patients with stage I, II, or III breast cancer. N Engl J Med, 2000. 342(8): p. 525–33. [PubMed: 10684910]
2. Schardt JA, et al. , Genomic analysis of single cytokeratin-positive cells from bone marrow reveals early mutational events in breast cancer. Cancer Cell, 2005. 8(3): p. 227–39. [PubMed: 16169467]
3. Werner-Klein M, et al. , Genetic alterations driving metastatic colony formation are acquired outside of the primary tumour in melanoma. Nat Commun, 2018. 9(1): p. 595. [PubMed: 29426936]
4. Hu Z, et al. , Quantitative evidence for early metastatic seeding in colorectal cancer. Nat Genet, 2019. 51(7): p. 1113–1122. [PubMed: 31209394]

5. Sanger N, et al. , Disseminated tumor cells in the bone marrow of patients with ductal carcinoma in situ. Int J Cancer, 2011. 129(10): p. 2522–6. [PubMed: 21207426]
6. Hosseini H, et al. , Early dissemination seeds metastasis in breast cancer. Nature, 2016.
7. Harper KL, et al. , Mechanism of early dissemination and metastasis in Her2(+) mammary cancer. Nature, 2016.
8. Narod SA, et al. , Breast Cancer Mortality After a Diagnosis of Ductal Carcinoma In Situ. JAMA Oncol, 2015. 1(7): p. 888–96. [PubMed: 26291673]
9. Rhim AD, et al. , EMT and dissemination precede pancreatic tumor formation. Cell, 2012. 148(1-2): p. 349–61. [PubMed: 22265420]
10. Linde N, et al. , Macrophages orchestrate breast cancer early dissemination and metastasis. Nat Commun, 2018. 9(1): p. 21. [PubMed: 29295986]
11. Hu Z, et al. , Multi-cancer analysis of clonality and the timing of systemic spread in paired primary tumors and metastases. Nat Genet, 2020.
12. Roses RE, et al. , Ductal carcinoma-in-situ of the breast with subsequent distant metastasis and death. Ann Surg Oncol, 2011. 18(10): p. 2873–8. [PubMed: 21476105]
13. Sosa MS, et al. , NR2F1 controls tumour cell dormancy via SOX9- and RARbeta-driven quiescence programmes. Nat Commun, 2015. 6: p. 6170. [PubMed: 25636082]
14. Adam AP, et al. , Computational identification of a p38SAPK-regulated transcription factor network required for tumor cell quiescence. Cancer Res, 2009. 69(14): p. 5664–72. [PubMed: 19584293]
15. Brancho D, et al. , Mechanism of p38 MAP kinase activation in vivo. Genes Dev, 2003. 17(16): p. 1969–78. [PubMed: 12893778]
16. Gunther EJ, et al. , A novel doxycycline-inducible system for the transgenic analysis of mammary gland biology. FASEB J, 2002. 16(3): p. 283–92. [PubMed: 11874978]
17. Moody SE, et al. , Conditional activation of Neu in the mammary epithelium of transgenic mice results in reversible pulmonary metastasis. Cancer Cell, 2002. 2(6): p. 451–61. [PubMed: 12498714]
18. Schneider CA, Rasband WS, and Eliceiri KW, NIH Image to ImageJ: 25 years of image analysis. Nat Methods, 2012. 9(7): p. 671–5. [PubMed: 22930834]
19. Entenberg D, et al. , Time-lapsed, large-volume, high-resolution intravital imaging for tissue-wide analysis of single cell dynamics. Methods, 2017. 128: p. 65–77. [PubMed: 28911733]
20. Entenberg D, et al. , Setup and use of a two-laser multiphoton microscope for multichannel intravital fluorescence imaging. Nat Protoc, 2011. 6(10): p. 1500–20. [PubMed: 21959234]
21. Behbod F, et al. , An intraductal human-in-mouse transplantation model mimics the subtypes of ductal carcinoma in situ. Breast Cancer Res, 2009. 11(5): p. R66. [PubMed: 19735549]
22. Wolff AC, et al. , American Society of Clinical Oncology/College of American Pathologists guideline recommendations for human epidermal growth factor receptor 2 testing in breast cancer. J Clin Oncol, 2007. 25(1): p. 118–45. [PubMed: 17159189]
23. Wen H-C, et al. , p38alpha Signaling Induces Anoikis and Lumen Formation During Mammary Morphogenesis. Sci. Signal, 2011. 4(174): p. ra34. [PubMed: 21610252]
24. Wang J, et al. , Her2 promotes early dissemination of breast cancer by suppressing the p38-MK2-Hsp27 pathway that is targetable by Wip1 inhibition. Oncogene, 2020. 39(40): p. 6313–6326. [PubMed: 32848211]
25. Barnabas N and Cohen D, Phenotypic and Molecular Characterization of MCF10DCIS and SUM Breast Cancer Cell Lines. Int J Breast Cancer, 2013. 2013: p. 872743. [PubMed: 23401782]
26. Miwatashi S, et al. , Novel inhibitor of p38 MAP kinase as an anti-TNF-alpha drug: discovery of N-[4-[2-ethyl-4-(3-methylphenyl)-1,3-thiazol-5-yl]-2-pyridyl]benzamide (TAK-715) as a potent and orally active anti-rheumatoid arthritis agent. J Med Chem, 2005. 48(19): p. 5966–79. [PubMed: 16162000]
27. Pickens BS, et al. , Role of COUP-TFI during retinoic acid-induced differentiation of P19 cells to endodermal cells. J Cell Physiol, 2013. 228(4): p. 791–800. [PubMed: 23018522]
28. Rada-Iglesias A, et al. , Epigenomic annotation of enhancers predicts transcriptional regulators of human neural crest. Cell Stem Cell, 2012. 11(5): p. 633–48. [PubMed: 22981823]

29. Adam F, et al. , COUP-TFI (chicken ovalbumin upstream promoter-transcription factor I) regulates cell migration and axogenesis in differentiating P19 embryonal carcinoma cells. Mol Endocrinol, 2000. 14(12): p. 1918–33. [PubMed: 11117523]
30. Alfano C, et al. , COUP-TFI promotes radial migration and proper morphology of callosal projection neurons by repressing Rnd2 expression. Development, 2011. 138(21): p. 4685–97. [PubMed: 21965613]
31. Hong Y, et al. , Mouse-INtraDuctal (MIND): an in vivo model for studying the underlying mechanisms of DCIS malignancy. J Pathol, 2021.
32. Fazilaty H, et al. , A gene regulatory network to control EMT programs in development and disease. Nat Commun, 2019. 10(1): p. 5115. [PubMed: 31712603]
33. Luck AA, et al. , The influence of basal phenotype on the metastatic pattern of breast cancer. Clin Oncol (R Coll Radiol), 2008. 20(1): p. 40–5. [PubMed: 17981444]
34. Evans AJ, et al. , Basal phenotype: a powerful prognostic factor in small screen-detected invasive breast cancer with long-term follow-up. J Med Screen, 2007. 14(4): p. 210–4. [PubMed: 18078567]
35. Cheung KJ, et al. , Collective invasion in breast cancer requires a conserved basal epithelial program. Cell, 2013. 155(7): p. 1639–51. [PubMed: 24332913]
36. Wang G, et al. , Her2 promotes early dissemination of breast cancer by suppressing the p38 pathway through Skp2-mediated proteasomal degradation of Tpl2. Oncogene, 2020. 39(47): p. 7034–7050. [PubMed: 32989258]
37. Sanchez-Tillo E, et al. , ZEB1 represses E-cadherin and induces an EMT by recruiting the SWI/SNF chromatin-remodeling protein BRG1. Oncogene, 2010. 29(24): p. 3490–500. [PubMed: 20418909]
38. Vesuna F, et al. , Twist is a transcriptional repressor of E-cadherin gene expression in breast cancer. Biochem Biophys Res Commun, 2008. 367(2): p. 235–41. [PubMed: 18062917]
39. Takano S, et al. , Prrx1 isoform switching regulates pancreatic cancer invasion and metastatic colonization. Genes Dev, 2016. 30(2): p. 233–47. [PubMed: 26773005]
40. Shamir ER, et al. , Twist1-induced dissemination preserves epithelial identity and requires E-cadherin. J Cell Biol, 2014. 204(5): p. 839–56. [PubMed: 24590176]
41. Pastushenko I, et al. , Identification of the tumour transition states occurring during EMT. Nature, 2018. 556(7702): p. 463–468. [PubMed: 29670281]
42. Fluegen G, et al. , Phenotypic heterogeneity of disseminated tumour cells is preset by primary tumour hypoxic microenvironments. Nat Cell Biol, 2017. 19(2): p. 120–132. [PubMed: 28114271]
43. Borgen E, et al. , NR2F1 stratifies dormant disseminated tumor cells in breast cancer patients. Breast Cancer Res, 2018. 20(1): p. 120. [PubMed: 30322396]
44. Chery L, et al. , Characterization of single disseminated prostate cancer cells reveals tumor cell heterogeneity and identifies dormancy associated pathways. Oncotarget, 2014. 5(20): p. 9939–51. [PubMed: 25301725]
45. Smits BM, et al. , The gene desert mammary carcinoma susceptibility locus Mcs1a regulates Nr2f1 modifying mammary epithelial cell differentiation and proliferation. PLoS Genet, 2013. 9(6): p. e1003549. [PubMed: 23785296]

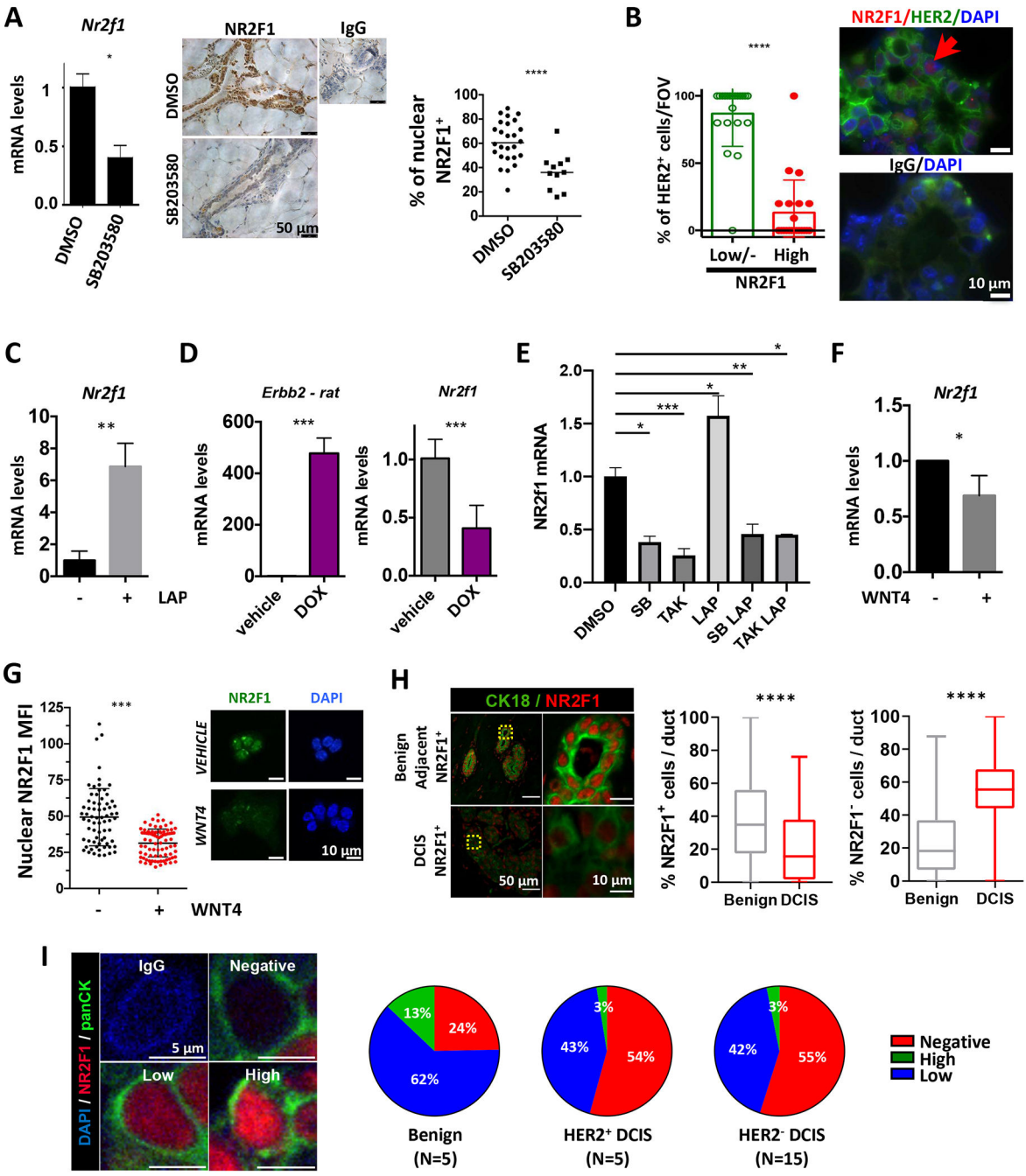

Figure 1. NR2F1 is downstream of p38 and HER2 signaling in ECCs.

A. QPCR and percentage of cells/duct with nuclear NR2F1 shown by IHC from mammary glands of MMTV-HER2 females treated with SB203580. N=2 mice/condition. **B.** Percentage of HER2 positive^{+} cells per field of view (FOV) that has either NR2F1^{HIGH} or NR2F1$^{LOW/NEGATIVE}$ expression in young MMTV-HER2 mammary glands by IF. 21 random fields, N=2 mice/condition. **C.** QPCR for *Nr2f1* in MMTV-HER2 ECC sphere cultures treated with Lapatinib. N=3. **D.** QPCR for *Erbb2* and *Nr2f1* in acini derived from MMTV-rtTA/TetO-NeuNT MECs after DOX induction. N=2. **E.** QPCR for *Nr2f1*

in MMTV-HER2 ECCs **in 2D** after treatment with SB203580 or TAK715, alone or in combination with Lapatinib. N=2. **F&G**. *Nr2f1* expression by QPCR (**F**) and IF (**G**) in MMTV-HER2 ECC after treatment with rWNT4. N=2. **H&I.** IF for CK18 and NR2F1 in 20 DCIS patients. Percentage of nuclear $NR2F1^{+}$ and $NR2F1^{-}$ cells/duct is shown (**H**). Percentage of cells with nuclear $NR2F1^{HIGH}$, $NR2F1^{LOW}$ and $NR2F1^{NEGATIVE}$ per duct/lesion in DCIS HER2+ or HER2− samples (**I**). For all graphs, mean (dotplot) or mean±SD (bar graphs) is shown and student's unpaired t- test, except **A, B&G** Mann-Whitney test and H Fisher's exact test.

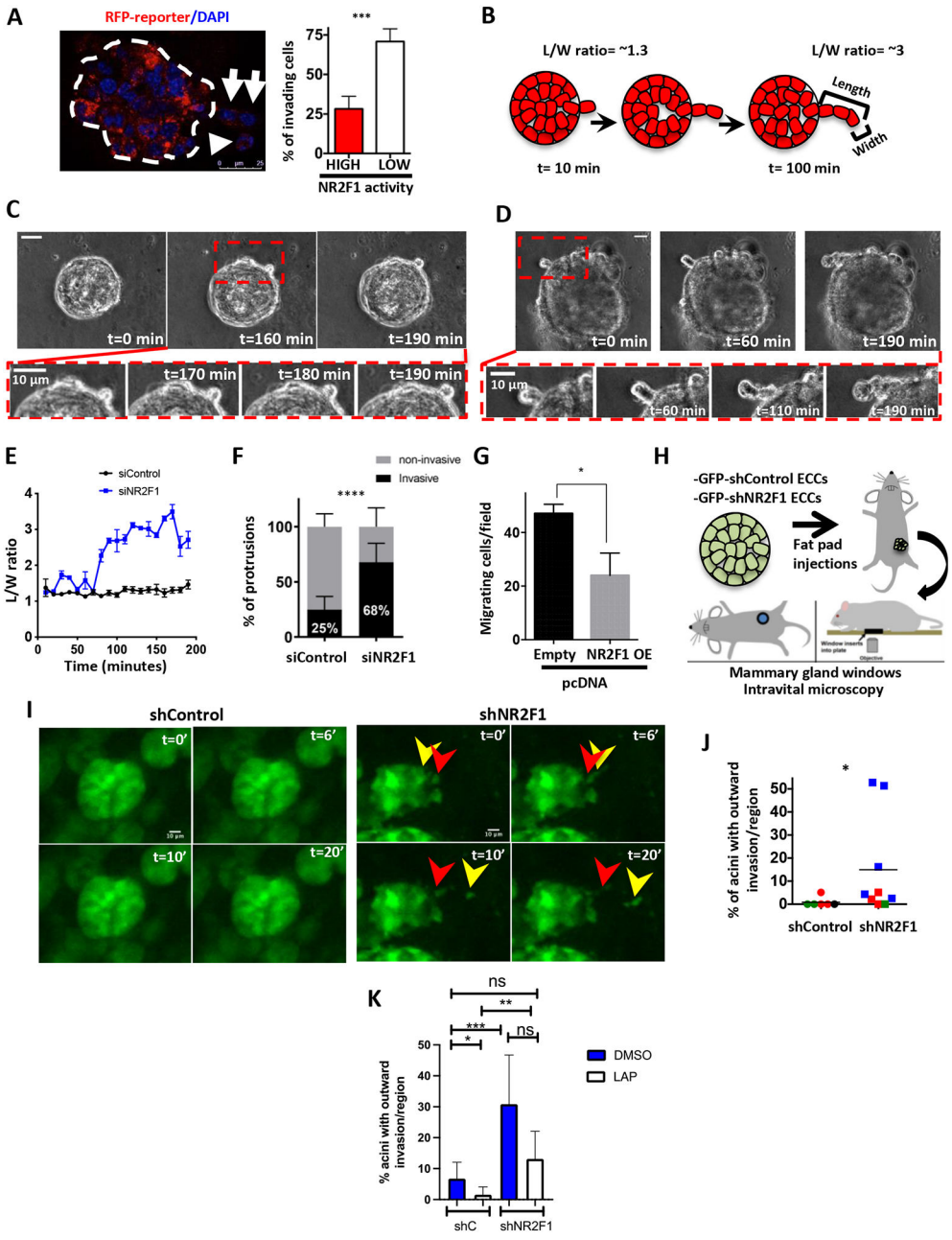

Figure 2. NR2F1 inhibits MMTV-HER2 ECCs invasion.

A. Percentage of invading cells with high/low NR2F1 reporter activity in acini by IF. Arrows show invading cells. **B.** Schematic of invasive protrusions and length-over-width (L/W) ratio. **C&D.** Time lapse imaging of siControl (C) or siNR2F1 (D) acini. **E.** L/W ratio of protrusions in siControl (black) or si*Nr2f1* (blue) acini. **F.** Percentage of invasive and non-invasive protrusions in siControl and si*Nr2f1* in acini. N=2. Fisher's exact test. **G.** Migration assay for NR2F1-overexpressing or empty vector control MMTV-HER2 ECCs. N=2. **H.** Schematic of intravital imaging using mammary gland windows (Adapted[19]). **I&J.** Percentage of acinar structures with outward invasion (J) by intravital imaging (I) in mice orthotopically injected with shControl or sh*Nr2f1* MMTV-HER2 ECCs. N=3-4mice/

group (colored). **K.** Percentage of acinar structures with outward invasion by intravital imaging in mice injected with same cells as in J and treated with lapatinib for 48 h. N=2-4 mice/group. For all graphs, mean (dotplot) or mean±SD (bar graphs) is shown and student's unpaired t- test, Mann-Whitney test (for J&K), unless otherwise noted.

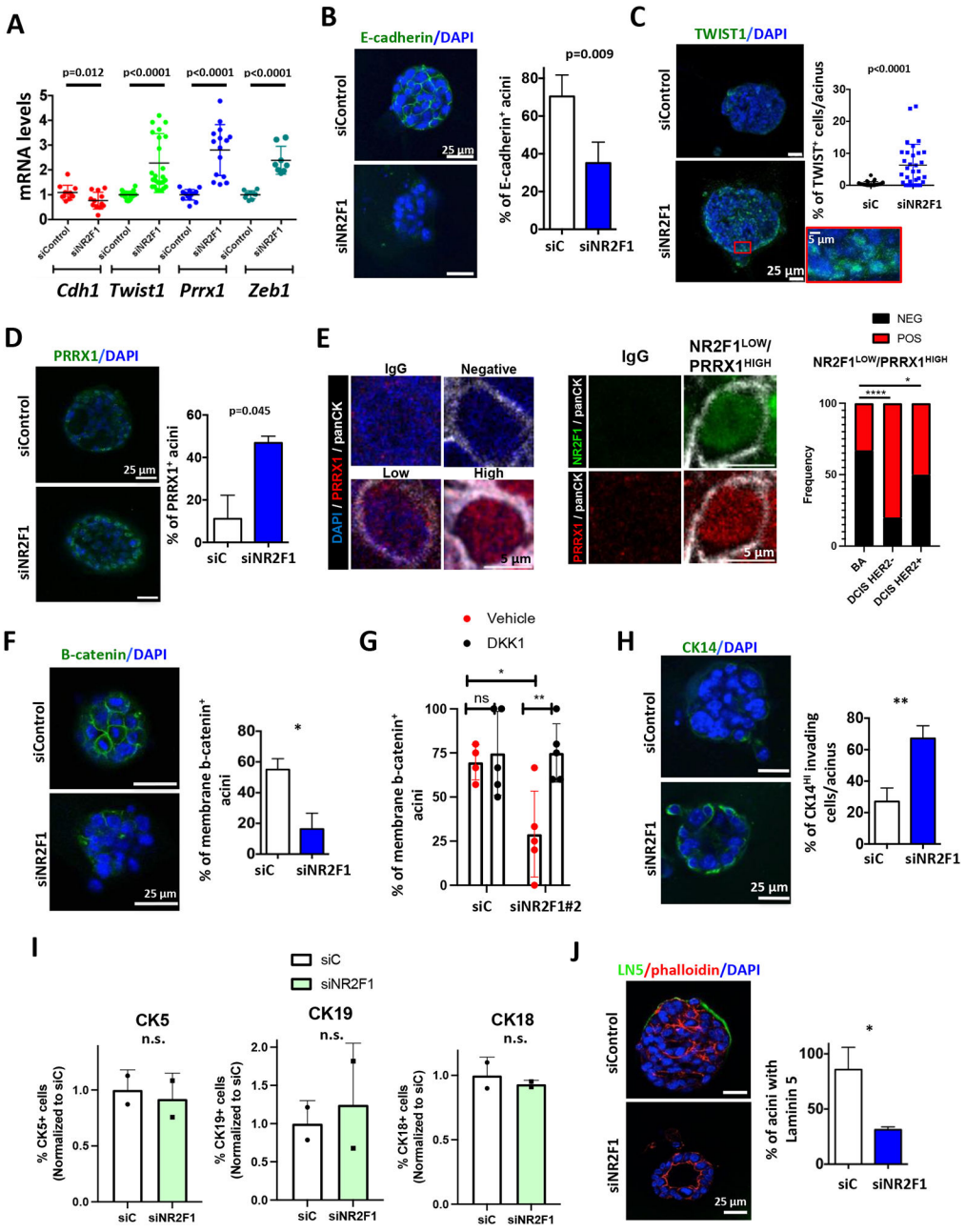

Figure 3. NR2F1 depletion allows a partial EMT and hybrid luminal/basal program in MMTV-HER2 ECC acini.

A. QPCR for the indicated genes in siControl vs. si*Nr2f1* MMTV-HER2 ECC acini. N=3-9. **B**. Percentage of E-cadherin+ acini by IF. N=3. **C**. Percentage of TWIST1+ cells per acinus. N=2. **D.** Percentage of PRRX1+ acini by IF. N=2. **E.** IF staining for NR2F1 (green), PRRX1 (red) and panCK (gray) in HER2− (n=6), HER2+ (n=7) and benign adjacent (n=6) DCIS samples. Representative images for PRRX1 levels are shown (left). Representative cell with NR2F1^{LOW}/PRRX1^{HIGH} signature is shown (middle). Fisher's exact test. **F**. Percentage of β-catenin+ MMTV-HER2 ECC acini by IF after transfection with siRNA. N=2. **G.** Percentage of β-catenin+ acini after transfection with si*Nr2f1*#2 and treatment with rDKK1.

N=2. **H**. Percentage of CK14+ invading cells per acinus. N=2. **I**. Luminal and basal marker expression by FC in acini from freshly isolated MMTV-HER2 ECCs. N=2. **J.** Percentage of laminin V+ acini by IF. N=2. For all graphs, mean (dotplot) or mean±SD (bar graphs) is shown and student's unpaired t- test, unless otherwise noted.

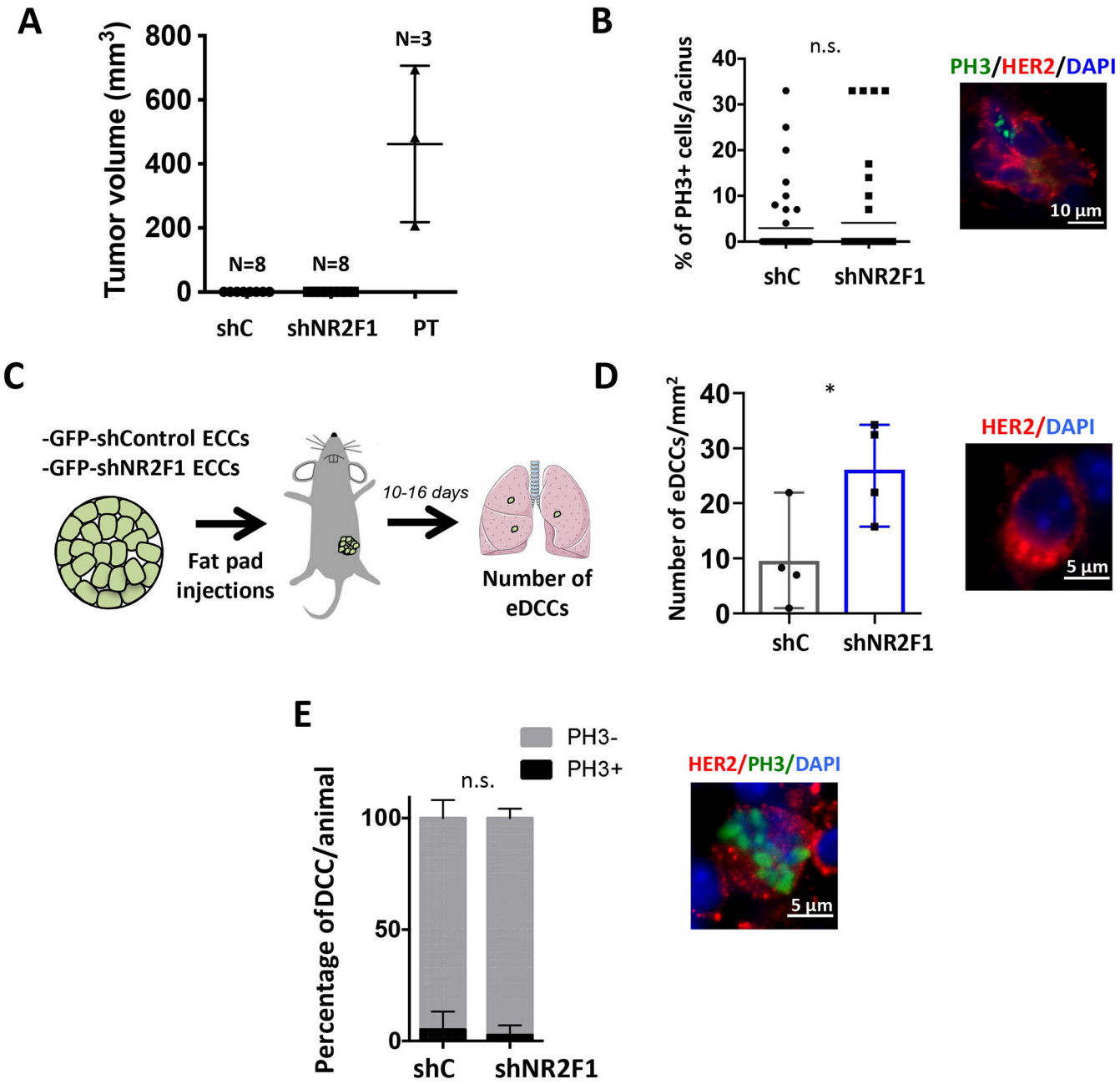

Figure 4. NR2F1 inhibits systemic dissemination of MMTV-HER2 ECCs.

A. Tumor volume measurements in nude mice orthotopically injected with shControl and sh*Nr2f1* MMTV-HER2 ECCs or MMTV-HER2 tumor-derived (PT) cells. **B.** Percentage of PH3+ cells/acinus in mammary glands orthotopically injected with shControl or sh*Nr2f1* MMTV-HER2 ECCs 10-16 day post-injections. N=2 mice/group. **C.** Experimental design for detection of eDCCs in nude mice 10-16 days after ortothopic injection with shControl and sh*Nr2f1* MMTV-HER2 ECCs. N=4mice/group. **D.** Number of eDCCs (HER2+) per lung area as described in C. Number of DCCs= 4,399 shControl; 4,305 sh*Nr2f1*. Representative image shown, scale bar=5 µm. **E.** Percentage of PH3+/HER2+ lung eDCCs as described in C. Number of eDCCs= 4,399 shControl; 4,305 sh*Nr2f1*. Image depicts a

PH3+ eDCCs, scale bar=5 μm. For all graphs, mean (dotplot) or mean±SD (bar graphs) is shown and student's unpaired *t*- test, unless otherwise noted.

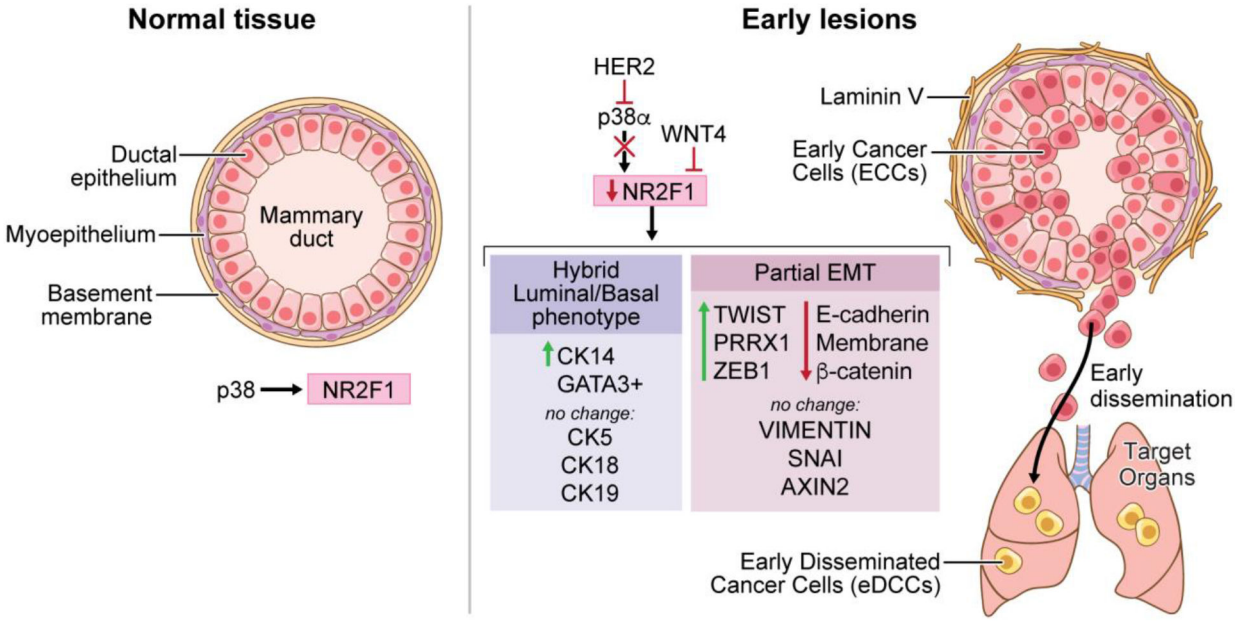

Figure 5. Graphical summary.

Our data suggest that p38 inactivity reduces NR2F1 levels in normal mammary epithelial cells (left) and MMTV-HER2 ECCs (right). In the latter scenario, NR2F1 downregulation led to a partial EMT, a shift β-catenin localization from membrane to nuclei and a hybrid luminal/basal phenotype allowing dissemination of ECCs to distant organs. Thus, NR2F1 acts as a barrier for early dissemination and its loss in early lesions could indicate the presence of early disseminated cancer cells (eDCCs). Image by Jill Gregory. Used with permission of ©Mount Sinai Health System.